

Functionalized Graphdiyne Nanowires: On-Surface Synthesis and Assessment of Band Structure, Flexibility, and Information Storage Potential

Florian Klappenberger,* Raphael Hellwig, Ping Du, Tobias Paintner, Martin Uphoff, Liding Zhang, Tao Lin, Bahare Abedin Moghanaki, Mateusz Paszkiewicz, Ivana Vobornik, Jun Fujii, Olaf Fuhr, Yi-Qi Zhang, Francesco Allegretti, Mario Ruben, and Johannes V. Barth

Carbon nanomaterials exhibit extraordinary mechanical and electronic properties desirable for future technologies. Beyond the popular sp^2 -scaffolds, there is growing interest in their graphdiyne-related counterparts incorporating both sp^2 and sp bonding in a regular scheme. Herein, we introduce carbonitrile-functionalized graphdiyne nanowires, as a novel conjugated, one-dimensional (1D) carbon nanomaterial systematically combining the virtues of covalent coupling and supramolecular concepts that are fabricated by on-surface synthesis. Specifically, a terphenylene backbone is extended with reactive terminal alkyne and polar carbonitrile (CN) moieties providing the required functionalities. It is demonstrated that the CN functionalization enables highly selective alkyne homocoupling forming polymer strands and gives rise to mutual lateral attraction entailing room-temperature stable double-stranded assemblies. By exploiting the templating effect of the vicinal Ag(455) surface, 40 nm long semiconducting nanowires are obtained and the first experimental assessment of their electronic band structure is achieved by angle-resolved photoemission spectroscopy indicating an effective mass below $0.1m_0$ for the top of the highest occupied band. Via molecular manipulation it is showcased that the novel oligomer exhibits extreme mechanical flexibility and opens unexplored ways of information encoding in clearly distinguishable CN-phenyl *trans-cis* species. Thus, conformational data storage with density of 0.36 bit nm^{-2} and temperature stability beyond 150 K comes in reach.

Carbon-based materials exhibit extraordinary mechanical and electronic properties. They are a central research topic in the 21st century and promising candidates for future nanotechnology applications. A plethora of nanomaterials is based on established sp^2 -hybridized scaffolds such as carbon nanotubes

(CNTs),^[1] graphene sheets,^[2] and graphene nanoribbons.^[3,4] Recently, significant interest in their graphyne and graphdiyne-related counterparts incorporating both sp^2 - and sp -hybridized carbon atoms is quickly emerging.^[5–8] Notably, theoretical investigations predict promising characteristics suitable for a broad variety of applications including molecular electronics, energy storage, gas filtering, and light harvesting.^[9–13] However, the experimental realization of the targeted materials remains challenging and, so far, solution-based synthesis approaches only afforded multilayered materials with significant amounts of impurities and unknown structural properties.^[14]

Various routes to the fabrication of high-quality carbon materials are currently being investigated,^[15] of which the epitaxial growth on well-defined metal substrates under ultrahigh vacuum (UHV) conditions is considered one of the most promising. Combining it with the covalent on-surface synthesis from rationally designed organic precursors^[16] paved the way to the engineering of stable^[17] and atom-precise nanostructures,^[18] amongst them various types of conjugated polymer wires^[19–21] and graphene nanoribbons.^[4,18,22,23]

them various types of conjugated polymer wires^[19–21] and graphene nanoribbons.^[4,18,22,23]


In this context, the homocoupling reaction of terminal alkyne tectons has raised great hopes for the construction of graphdiyne-related nanostructures.^[8,24,25] However, the intricate

Dr. F. Klappenberger, Dr. R. Hellwig, T. Paintner, M. Uphoff, L. Zhang, Dr. T. Lin, B. Abedin Moghanaki, M. Paszkiewicz, Dr. Y.-Q. Zhang, Dr. F. Allegretti, Prof. J. V. Barth
 Physik-Department E20
 Technische Universität München
 85748 Garching, Germany
 E-mail: florian.klappenberger@tum.de

Dr. P. Du, Dr. O. Fuhr, Prof. M. Ruben
 Institute für Nanotechnologie
 Karlsruher Institut für Technologie (KIT)
 76344 Eggenstein-Leopoldshafen, Germany

Dr. I. Vobornik, Dr. J. Fujii
 Istituto Officina dei Materiali (IOM)-CNR
 Laboratorio TASC
 Area Science Park, I-34149 Trieste, Italy

Prof. M. Ruben
 IPCMS-CNRS
 Université de Strasbourg
 F-67034 Strasbourg, France

 The ORCID identification number(s) for the author(s) of this article can be found under <https://doi.org/10.1002/sml.201704321>.

DOI: 10.1002/sml.201704321

coupling mechanism^[24,26] and the occurrence of cross-linking side reactions^[27] prevented so far the production of high-quality 2D architectures. With the help of substrate templating mechanisms, which proved efficient for increasing regio- and chemoselectivity,^[28–31] so-called extended graphdiyne (GDY) nanowires were realized on a vicinal surface.^[32] Since the unit cell contained three phenyl and two alkyne moieties, the specific nanowire is designated a 3-2 GDY nanowire. Although these efforts demonstrate that novel carbon-based materials are within reach, improved control and optimized synthesis protocols are required to obtain organic semiconductor nanostructures and materials with high quality in technologically relevant quantities.

Here, we introduce functionalized graphdiyne (f-GDY) nanowires as promising novel nanomaterial rendered possible by controlled synthesis via surface-confined coupling of specifically designed precursors on well-defined silver surfaces under UHV conditions (cf. schematic illustration in **Figure 1a**). Through the complementary insights of scanning tunneling microscopy (STM) with photoelectron spectroscopy (PES)^[33] we comprehensively assess their electronic and mechanical properties. We contrast the original linear diethynyl-terphenyl precursor (DETP, **Figure 1b**) carrying only the reactive alkynes as primary functional groups responsible for covalent coupling with its de novo synthesized derivative compound (CN-DETP, **Figure 1c**) implementing additional carbonitrile (CN) moieties as secondary functional groups with decisive impact. We find that the improved precursor design not only significantly increases the selectivity of the targeted alkyne homocoupling reaction but also generates supramolecular interactions between the nanowires thereby forming double- and multiple-stranded assemblies stable at room temperature (RT). In combination with the templating effect of a vicinal surface, we achieve 40 nm long oligomeric strands and confirm the theoretical electronic band structure predictions for the approximately cosine-shaped highest occupied band (HOB) of the 1D semiconductor by means of angle-resolved PES (ARPES). Finally, via STM tip manipulation procedures, we demonstrate information encoding with ultimate density by conformational *trans-cis* switching of individual conformers.

We developed a synthetic route to functionalized terminal alkyne precursors as described in detail in the Supporting Information. Following growth of a single crystal, the X-ray crystal structure analysis (**Figure S6**, Supporting Information) indicated a molecular arrangement that can be rationalized by supramolecular interactions mediated by the terminal alkyne and the CN groups. **Figure 1d** depicts a view where one can identify a self-complementary binding motif between two ethynyl-benzonitrile (EBN) moieties including two hydrogen bonds between the CN and the alkyne groups (dashed) which appears as a novel synthon for molecular crystal engineering (**Figure 1e**). Both N···H distances *D* amount to 2.48 Å, suggesting weak H-bonding. An energy optimization of a two EBN molecule cluster was performed to characterize the synthon (**Figure S7**, Supporting Information). For this ideal situation, a binding energy of 0.3 eV per synthon and a N···H distance of 2.2 Å is predicted by the density functional theory (DFT) calculations. In the real

3D crystal, additional weak electrostatic interactions between the nitrogen atoms of the CN groups and the adjacent phenyl rings of a third molecule interfere.^[34] The related N···H

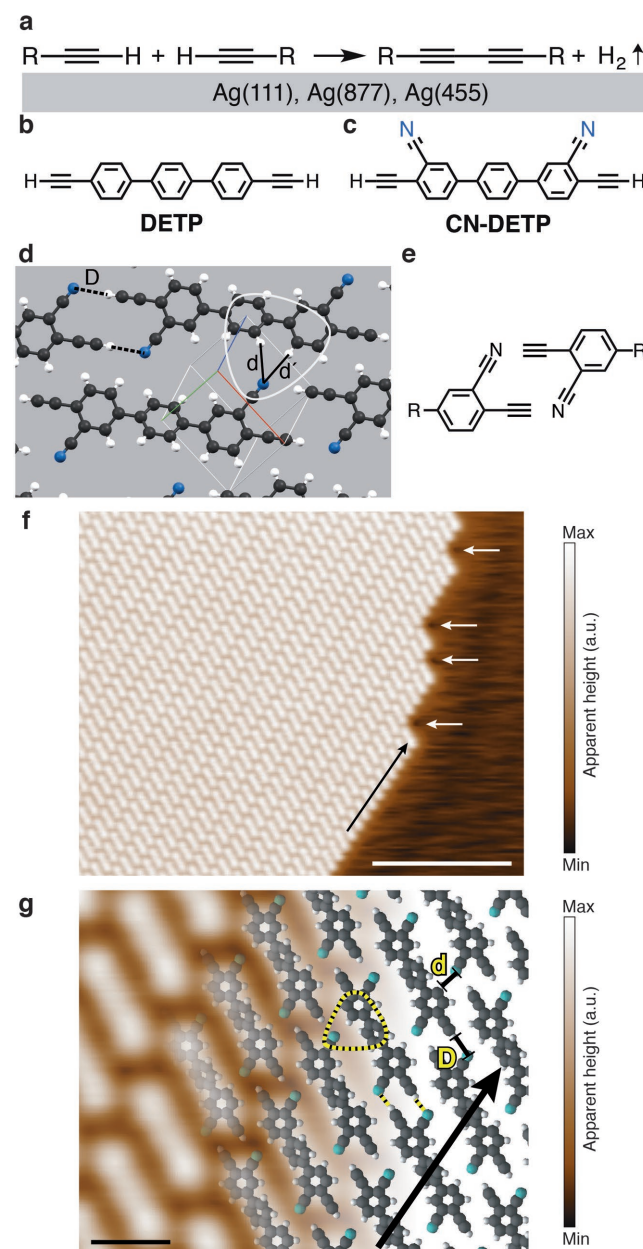


Figure 1. Coupling reaction, precursors, and novel synthon. a) On-surface homocoupling of terminal alkynes resulting in a linear butadiyne connection. b) Original diethynyl-terphenyl (DETP) precursor. c) De novo synthesized CN-functionalized diethynyl-terphenyl (CN-DETP) precursor. d) X-ray crystal structure data of CN-DETP. The view highlights the self-complementary head-to-tail binding motif connecting the ethynyl and nitrile groups (dashed lines) and the weak electrostatic interactions between the N atoms and neighboring phenyl rings (solid outline). e) Scheme of the novel ethynyl-benzonitrile synthon. f) Large-scale STM topograph ($I_T = 0.1$ nA, $V_B = -0.5$ V, scale bar 100 Å) showing a regular domain after deposition of CN-DETP onto the substrate held at room temperature. White arrows mark depressions. g) Close-up STM image ($I_T = 0.05$ nA, $V_B = -5$ mV, scale bar 10 Å) with molecular models superposed.

distances d and d' (Figure 1d) are 2.73 and 2.75 Å, respectively, typical values for this interaction.

We tested the chemical integrity of CN-DETP after the organic molecular beam epitaxy (OMBE) process by evaporation of a submonolayer coverage onto Ag(111) held at RT. In the STM data recorded at 5 K, extended and long-range ordered domains are observed (Figure 1f). The uniformity of the appearance of the individual molecular units indicates successful sublimation of intact CN-DETP. The analysis of the structural arrangement within a single domain (Figure 1g) evidences supramolecular binding motifs very similar to the crystal phase, clearly revealing the role of the functional groups on the precursor organization. Thereby, the systematic appearance of depressions (white arrows) at the right-top end of molecular chains (black arrows in panels f and g) indicates secondary functional group pointing outward.

In the following, we investigate the impact of the secondary functional group on the on-surface coupling process. For comparison, we first annealed a submonolayer coverage of DETP on Ag(111) at 400 K for 10 min. The STM data (Figure 2a) evidence polymeric wires of irregular shape resulting from a mixture of the targeted linear coupling (green circles) with twofold connections with varying bending angles (black) and a variety of threefold covalent linking motifs (red). Additionally, some connections with a sphere-shaped protrusion between monomers (blue) are consistent with the expected geometry and appearance of Ag bis-acetylides.^[24,35] Specifically, the large number of branched covalent connections obstructs the fabrication of linear, 1D nanowires with a precise structure. In contrast, when C–C coupling is initiated for CN-DETP under the same conditions (Figure 2b), a significantly improved linking behavior is observed. The majority of monomers are involved in straight and well-defined polymer segments, whereas deviations from linear coupling occur almost exclusively in the form of 90° bending. Moreover, polymeric strands often form double-wire assemblies resulting from the CN interactions. A large-scale STM image (Figure 2c) demonstrates that also bundles of aligned nanowires, lying parallel over distances up to 200 Å are formed. A statistical evaluation of an extensive data set demonstrates the significant increase in chemoselectivity toward linear homocoupling of alkyne groups, largely suppressing the various side reactions (Figure 2d). While DETP (red bars) succeeded in only 33%, the advanced precursor CN-DETP (blue bars) achieved 87%. For the latter compound, the branching covalent linkages (Figure 2d, threefold) are reduced to below 4% of the overall coupling events. Accordingly, our data demonstrate that precursor design incorporating specific secondary functional groups provides effective means towards enhanced control of covalent reaction pathways on the surface, improving the selectivity toward the desired coupling product. We suggest that steric repulsion due to the CN groups suppresses lateral access of terminal alkynes to the reactive butadiyne bridges, preventing branched coupling motifs. Although being weak, the supramolecular interactions between the nanowires might additionally promote the linear growth mode of the f-GDY polymer strands. Considering the electron withdrawing character of the CN moieties, also electronic effects could influence the coupling reaction, however dedicated investigations are required to unravel their roles.

Next, we inspect in more detail the precise nature of the polymerization products. The chemical structure of the 90° bending motif is unveiled by examining more closely a dimeric cluster of bent linkages (Figure 2e; Figure S8a,b, Supporting Information). It is associated with a side reaction where alkyne groups undergo a coupling and isomerization reaction without H abstraction, but where transfer of both H atoms onto an original alkyne has occurred, yielding an ethynyl-vinyl bridge. Superposing scaled models of two such 90° structures geometry-optimized in gas phase (see the Experimental Section) nicely matches the STM data. Supramolecular interactions are indicated by the antiparallel alignment of neighboring CN groups. Furthermore, the modeling demonstrates that the presence of depressions in the surrounding metal surface (black) is caused by the secondary functional groups pointing outward. Such depressions were consistently visualized for small negative bias voltages throughout our investigations (cf. Figures 1,4,5; Figure S8, Supporting Information). Related depressions have been reported before also for other functional groups featuring lone pairs such as pyridine,^[36] the carboxylate group,^[36] and deprotonated alkynes.^[37] The depressions were ascribed to local changes of the tunneling barrier via the lone pair generated surface dipoles.^[36]

Close inspection of a high-resolution image (Figure 2f; Figure S8c,d, Supporting Information) with intermolecular contrast reveals the structure of the double chains. Specifically, all building blocks exhibit a *cis* conformation enabling that the CN groups mediate lateral attraction between the individual wires of the double-stranded assembly. Furthermore, the antiparallel alignment of the polar groups results in the relative displacement of one covalent chain against the other along the main chain direction such that the butadiyne sections of one wire (marked blue) are lining up with the terphenyl sections of the second wire (marked red). Similar binding motifs have been observed before for a related carbonitrile-terphenyl species^[38] or in the double-strand formation with carboxylic acid units.^[39,40] A recent theoretical analysis^[41] quantified that each CN group contributes with a binding energy of around 0.1 eV. Accordingly, oligomeric double chain segments should exhibit a significant temperature stability due to accumulated interchain bonding. Indeed, when recording STM data at RT, the double and triple chain sections can be clearly identified (Figure S9, Supporting Information), and their shape and position remain unchanged over the time scale of the acquisition of several STM images (3 min per image).

Next, we evaluated the potential of optimizing the functionalized nanowire growth by exploiting the lateral patterning of a regular anisotropic surface.^[32] To this purpose, we employed the vicinal Ag(455) surface (Figure S10, Supporting Information), which consists of narrow terraces (average width = 23.35 Å) of the close-packed (111) facet and thus provides a high density of monatomic step edges. Evaporation of 0.2 monolayer of CN-DETP onto the stepped surface at 300 K results in supramolecular chains aligned along the step edges and residing at their lower side (Figure S11a, Supporting Information). These regular chains consist mainly of *trans* isomers head-to-tail connected similar to the crystal phase. A minority of *cis* isomers are also present, often where chains are disrupted. After

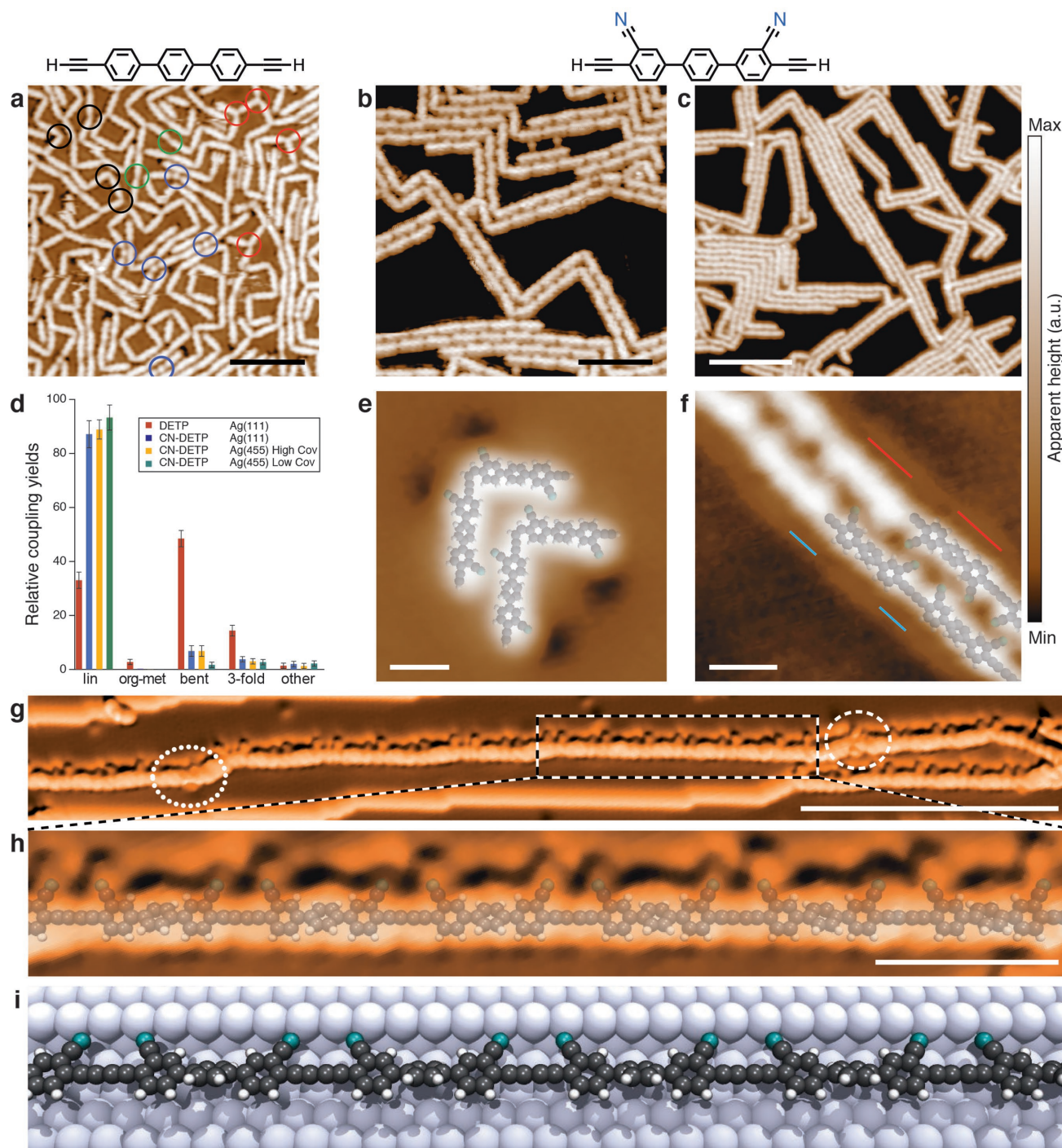


Figure 2. Fabrication of f-GDY nanowires. a) STM topograph ($I_T = 0.2$ nA, $V_B = -0.3$ V) of DETP on Ag(111) after annealing to 400 K. Besides the targeted linear coupling (green circles), distorted linkages (black circles), trifurcated motifs (red circles), and occasional bis-acetylide couplings (blue circles) occur. b,c,e,f) STM topographs (0.1 nA, -10 mV) of CN-DETP on Ag(111) after annealing to 400 K. Extended polymeric strands are present forming b) double lines and c) bundles. d) Relative yields of the different coupling reactions. Zoom-in image of e) an isolated, dimeric 90° bending motif and f) of the self-assembled double-strand structures with superimposed molecular models. g) STM image (0.09 nA, -0.9 V) of a 400 Å-long polymer strand fabricated on Ag(455). A conformational isomer (dotted) and a chemical impurity (dashed) are marked. h) Close-up image of the highlighted area in panel (g) with semitransparent molecular model superimposed. i) Graphical representation of f-GDY nanowire lying at a step edge. Scale bars are 50 Å in (a) and (b), 100 Å in (c) and (g), 10 Å in (e) and (f), and 20 Å in (h).

annealing to 400 K, well-defined single strands following the step edges are visible in the STM image (white arrows in Figure S11b, Supporting Information). The high resolution achieved

clearly allows identifying the CN moieties pointing toward the step edge and demonstrates the regular structure of the polymeric wires.

In addition, sometimes double-stranded structures are present (black arrows in Figures S11 and S12, Supporting Information) at $\approx 20\%$ of the covered step edges exhibiting a highly correlated nanowire growth mode (cf. Figures S12 and S13, Supporting Information). An example of a 40 nm long nanowire with sharp intramolecular contrast is depicted in Figure 2g. The high resolution demonstrates the atom-precise structure whereby individual phenyl rings and CN groups can be distinguished. Two irregularities (marked) were attributed via additional analysis (Figure S14, Supporting Information) to a conformational isomer (dotted circle) with a CN group pointing away from the steps and to the only chemical impurity (dashed circle) of that wire, respectively. The statistical evaluation of the coupling motifs observed on this sample (Figure 2d, green bars) highlights the high selectivity toward alkyne homocoupling ($>93\%$) achieved with the improved precursor on the Ag(455). However, since for CN-DETP the homocoupling selectivity is already high on the Ag(111) surface, a dedicated investigation yielding smaller statistical error bars would be required to decide if vicinal surface templating^[32] leads to a significant improvement under such conditions. When exploring the efficiency of this vicinal surface templating effect for aligning f-GDY nanowires in the high coverage regime, our data (Figure S15, Supporting Information) reveal still high selectivity (Figure 2d, yellow bars) but the degree of alignment is reduced. The single strand length that we achieved is comparable to that of graphene nanoribbons on Au(111)^[18] and Au(788)^[42,43] and exceeds by far the average length achieved for nanoribbons including molecularly defined heterojunctions.^[44]

According to theoretical predictions of their band structure, graphdiyne nanowires are a direct band gap semiconducting material with promisingly high charge carrier mobilities up to $10^5 \text{ cm}^2 \text{ V}^{-1} \text{ s}^{-1}$,^[32,45,46] however experimental evidence is lacking so far. Here, we employed ARPES to address the electronic structure of the HOB of the on-surface synthesized nanowires. After taking references of a clean Ag(455) and a multilayer sample (Figure S16, Supporting Information), we prepared a CN-DETP submonolayer sample by evaporation at $T_{\text{sub}} = 300 \text{ K}$ leading to the adsorption of intact monomers. **Figure 3a** displays the angle-integrated PES spectrum (dotted line). The highest occupied molecular orbital (HOMO) level is clearly discernible and is identified as a “flat” feature without energy dispersion in the corresponding ARPES spectrum (Figure 3b). Conversely, after triggering nanowire formation by annealing ($T_{\text{ann}} = 400 \text{ K}$), the HOMO peak appears significantly broadened with its maximum shifted toward the Fermi level (Figure 3a). In the ARPES band dispersion map (Figure 3c) recorded with the k -resolving direction along the step edges, the related HOB feature (white and light-blue area) indeed exhibits an angle-dependent structure with evident mirror symmetry with respect to the central emission angle of 2° . The latter deviates from zero, due to minor imperfections of the sample alignment in the polar angle direction.

For the interpretation of the data, it is helpful to plot the band structure in the angle-dependent spectrum. We calculated the width of the Brillouin zone (BZ) $k_{\text{BZ}} = 2\pi/p \approx 0.35 \text{ \AA}^{-1}$ by taking into account the periodicity along the nanowire of $p = 18.1 \text{ \AA}$, resulting from crystal structure bond lengths, and the kinetic energy of the center of the HOB feature, $E_{\text{kin}} = 23 \text{ eV}$.

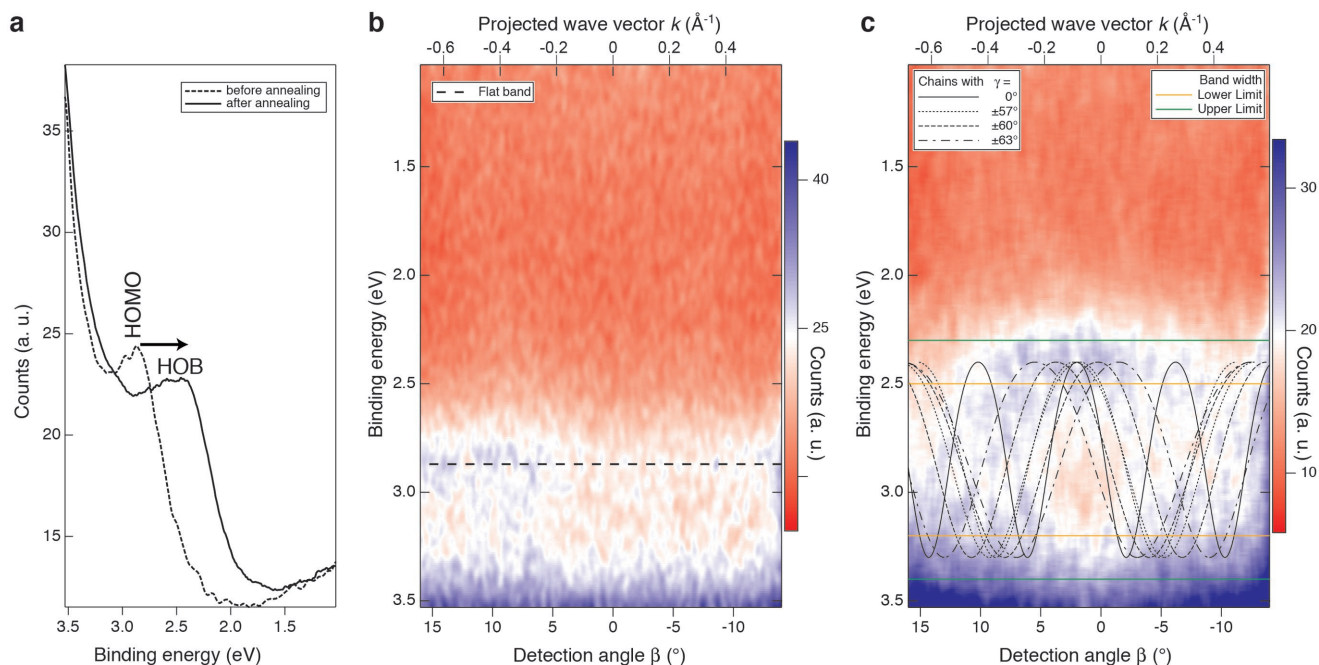


Figure 3. Assessment of the nanowire band structure via valence band photoelectron spectroscopy (PES). a) Angle-integrated PES spectra of a submonolayer of CN-DETP on Ag(455) before (dashed) and after annealing (solid) to 400 K. b) ARPES band dispersion map as a function of binding energy and emission angle before annealing. Superposed is a nondispersing feature expected for a flat band at the energy position of the HOMO. c) Same ARPES band dispersion map after annealing to 400 K. Superposed are the expected dispersion curves for 3-2 GDY nanowires with the denoted alignment with respect to the step direction and the upper and lower limits for the band width. In both panels (b) and (c), the projection of the electron wave vector onto the surface is aligned with the step edges.

The BZ width corresponds to an electron emission angle of 8.2° as obtained from the relation^[47] $k_{\parallel} = \frac{\sqrt{2m_0 E_{\text{kin}}}}{\hbar} \sin \alpha$, where

m_0 is the electron rest mass, k_{\parallel} the component of the wave vector of the emitted electron parallel to the step edge direction, and α the polar angle of emission. Figure 3c compares the expected dispersion (black solid line, cf. Figure S20, Supporting Information) with the experimental spectroscopic signature. Thereby, the energetic positioning of the theoretical bands was adjusted to fit the experimental alignment. Clearly, the broad observed structure cannot be explained with the single theoretical dispersion curve. The discrepancy is attributed to nonperfect alignment of the f-GDY strands as indicated by previous high coverage samples (cf. Figure S15, Supporting Information). For a more precise characterization, we carried out RT-STM investigation after the ARPES measurements on the very same sample. Indeed, the data (Figure S17a,b, Supporting Information) demonstrate that nanowires coexist aligned in various directions with respect to the step edges. As explained in the Supporting Information (Figures S18 and S19, Supporting Information), these nanowires, which have the same intrinsic band structure, but differ in their azimuthal alignment with respect to the k_{\parallel} -direction probed by the analyzer (i.e., along the step edges), contribute to the experimental ARPES spectrum with apparent dispersion curves strongly depending on the alignment angle. When adding the dispersion curves of the most often occurring alignment angles (0° and 60° allowing a 3° deviation due to imperfect alignment for the latter), the experimental signature of the HOB can be rationalized, which reinforces the high expectations put into such materials.

The overlapping dispersions prevent a direct evaluation of the effective mass, m_{eff} , at the top of the HOB. Therefore, we approximate the shape of the HOB by a cosine band

(cf. Figure S20, Supporting Information) and determine m_{eff} from the band width W . The data indicates that $W = 0.9 \pm 0.2$ eV. This value slightly exceeds the DFT predictions,^[32,45] but is well within the expected range. For a cosine-shaped dispersion the low field effective mass can be evaluated through the relation $m_{\text{eff}} = 2\hbar^2/(Wp^2)$.^[48] Taking into account the difference between the DFT-calculated band shape and the uncertainty in W (cf. Figure S20, Supporting Information), our analysis reveals that the hole effective mass amounts to between 0.06 and $0.1m_0$ at the top of the HOB. In comparison to 7-armchair graphene nanoribbons and polyphenylene nanowires, where effective masses between 0.21 and $0.17m_0$ were reported,^[43,49–51] the 3-2 GDY nanowire possesses a factor 2 to 3 smaller effective mass. Thus, under the assumption of comparable scattering rates, a significantly higher charge-carrier mobility should be achievable in f-GDY nanowires. According to a recent theoretical investigation,^[46] the GDY nanowire band structure can be tailored by secondary functionalization. Specifically, adding CN moieties to the original DETP precursor is predicted to pull down the HOB. Comparing PES data of DETP and CN-DETP samples (Figure S21, Supporting Information) we find a downshift of both the HOMO level of the isolated species and the HOB of the chains by 0.3 eV, well within the expected range. These findings demonstrate that intentional doping of f-GDY nanowires is possible by the choice of the secondary functional groups attached to the monomeric building blocks.

As exemplary illustration of tailored functionality, we explore the potential of conformational information encoding with the novel nanomaterial. Figure 4a depicts an STM topograph of an isolated f-GDY nanowire where the curved appearance of the dicarbonitrile-terphenyl units indicates that all CN-moieties are pointing to the right. Depressions (dark spots) in the apparent height of the metal surface are present on the right side of the wire. This is consistent with our earlier discussion

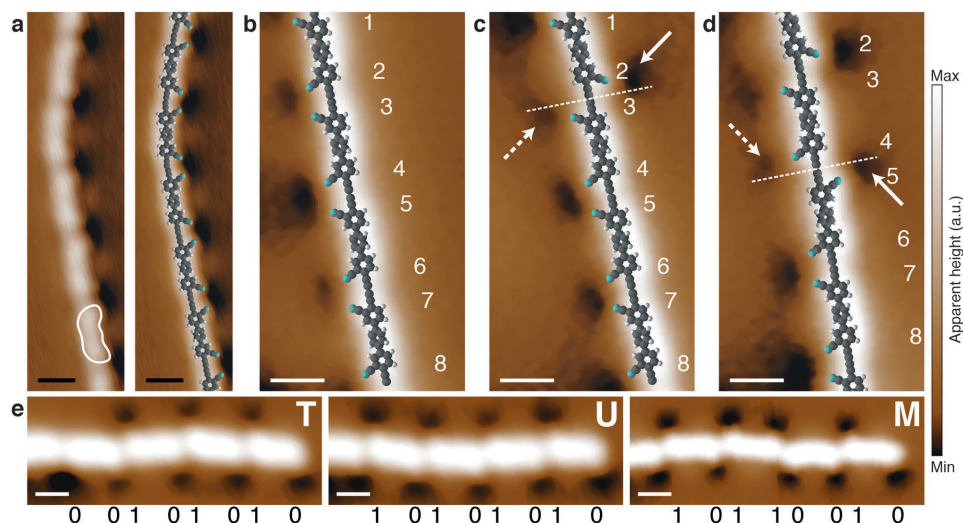


Figure 4. Conformational information storage. a) Isolated f-GDY wire with the curved appearance of monomeric units (highlighted) indicating the alignment of CN groups. Left panel: STM data, right panel: same data with molecular models. b) A short polymer sequence with only left-pointing CN moieties defined as “0”s. c) After the first tip manipulation, the second CN group is pointing to the right, i.e., was selectively switched to the “1” state (solid arrow). d) By the second tip manipulation, the fifth “bit” was switched, again without interfering with bit number 4. e) Different conformational states of the very same 5-monomer long nanowire with encoded 8-bit ASCII values 84, 85, and 77 representing the letters “T”, “U”, and “M”, respectively. For all topographs $I_T = 0.1$ nA, $V_B = -0.1$ V, and scale bars are 10 Å.

(Figures 1 and 2; Figure S8, Supporting Information) that the depressions are induced by the CN groups.

For demonstrating the possibility of selective switching we now focus on a tetramer section of an isolated single f-GDY nanowire, where we can assign eight bits to the individual positions of the CN groups (Figure 4b). For this system, we developed an STM tip manipulation procedure (see the Experimental Section) which allowed us to selectively switch individual CN-phenyl moieties between *trans* and *cis* states, see Figure 4c,d, where subsequently groups 2 and 5 were addressed, respectively. Thus, when assigning the bit values “0” and “1” to the conformational states at specific positions, f-GDY nanowires can be utilized for storing information of the CN moieties. As a further proof of the applicability of this novel polymeric information storage concept, we wrote the ASCII values of the letters “T”, “U”, and “M” subsequently into the very same pentameric end of a f-GDY nanowire (Figure 4e). With a periodicity of 18.2 Å along the molecular chain, two switchable conformers per monomer and a lateral extension of ≈ 3 nm, the storage density is 0.36 bit nm⁻². This value corresponds to 232 terabit per square inch, about two orders of magnitude larger than the storage density in recent hard disks. Noteworthy, the storage density we achieved outperforms antiferromagnetically coupled magnetic atom arrays^[52] by almost a factor of two. The barrier for a very similar isomerization process of the CN-phenyl moiety of a related meta-dicarbonitrile-terphenyl (CN₂-Ph₃) molecule was recently calculated to be ≈ 0.5 eV.^[53] For information storage with the long-term stability suited for technological applications usually a barrier of 40 $k_B T$ is required.^[54] Accordingly, a barrier of 0.5 eV would ensure reliable storage of information up to a temperature of 145 K. Taking into account

the increased molecule–substrate interaction in the case of an oligomeric f-GDY strand as compared to an individual CN₂-Ph₃ monomer, we can safely assume 145 K to be a lower limit for the real thermal stability of the conformational switches. Notably, this finding is in stark contrast to the very limited stability of the magnetic atom arrays becoming unstable at 4 K.^[52] Also, we exceed by far the most stable single atom magnets reported recently, where the magnetic remanence vanishes at 30 K.^[55] Furthermore, the expected energy barrier of more than half an eV for the conformational switching approach is almost twice as high as for the most recent information storage demonstrations utilizing Cl vacancy repositioning.^[56] Importantly, our approach includes the reversible switching between two states, thus naturally providing access to write and erase operations, tasks representing unsolved challenges for information-containing sequence-controlled polymers.^[57,58]

The capability of providing active components in flexible devices is one of the most important prospects of molecular electronics. Here, we tested the f-GDY nanowires regarding mechanical stability by STM tip manipulations. We prepared (cf. Figure S22, Supporting Information) a favorable situation with a unique marker next to a long polymer. In a stepwise procedure (Figure 5a to c), we detached the majority of the polymer from the step edge. In the resulting strongly distorted configuration (Figure 5d), an extremely small bending radius of 19 Å was achieved (red dashed circle). After a subsequent elongation (Figure 5e), a straight and fully intact f-GDY nanowire was obtained whereby the uniformity of the terphenyl and butadiyne subgroups and the CN-induced depressions reveal its unchanged structure. Similar investigation of surface-supported armchair graphene nanoribbons obtained a minimum

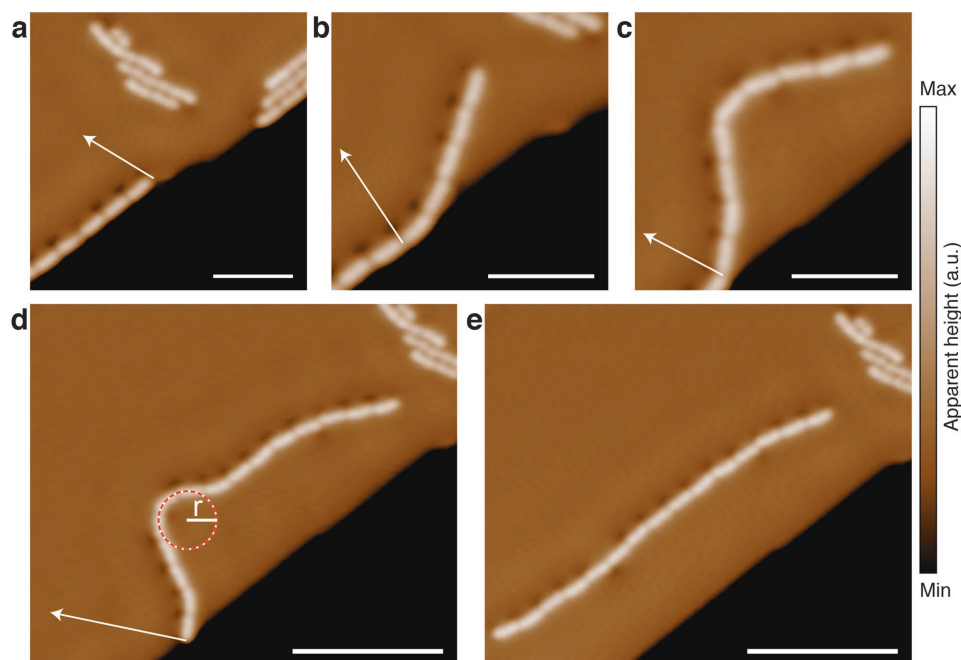


Figure 5. Extreme flexibility of a f-GDY nanowire. a–c) The upper right terminal part of a nanowire is step-wise pulled away from the step edge. d) After the previous manipulation step, the molecular wire exhibits a strongly bent conformation with bending radius $r = 19$ Å. e) After final detachment of the second end from the step edge, an almost straight configuration is restored. The scale bars in panels (a)–(c) and (d) and (e) are 50 and 100 Å, respectively. Scanning parameters are $I_T = 0.1$ nA, $V_B = 0.1$ V. Arrows represent the displacement of the tip in the manipulation mode.

bending radius of 28 nm before structural relaxations set in.^[59] Dedicated investigations for polyphenylene wires are missing, but available reports indicate bending radii around 6 nm.^[60] Polyfluorene^[19] and polythiophene^[21] wires can assume geometries with similarly large curvatures. However, these are established by conformational changes of the subunits featuring inherent angles without the necessity of actual bending bonds. As a drawback, bending and conformation-induced changes of the electronic properties are inherently linked.

In conclusion, we have constructed high-quality CN-functionalized 3-2 graphdiyne nanowires via on-surface covalent coupling of terminal alkyne building blocks. The secondary functional groups increased drastically the coupling efficiency, triggered the self-assembly nanowire bundles, acted as *n*-doping source, and allowed information storage via *trans*–*cis* conformer states with state-of-the-art storage density and unprecedented temperature stability. Our experimental band structure assessment evidences a significantly smaller effective mass than for graphene nanoribbons and polyphenylene nanowires and our mechanical characterization showcased extraordinary flexibility demonstrating that graphdiyne nanowires are perfectly suitable for flexible molecular electronics. Our results pave the way for a novel family of carbon-based materials comprising countless members due to combinatorial possibilities of its subunits, and with significant potential for nanotechnological applications.

Experimental Section

Synthesis: The 4,4′′-diethynyl-[1,1′:4′,1′′-terphenyl]-3,3′′-dicarbonitrile precursor (CN-DETP) was synthesized as described in the Supporting Information (see also Figure S1, Supporting Information). Multitechnique characterization (Figures S2–S5, Supporting Information) demonstrated the high purity of the obtained compound.

Sample Preparation: The experiments were carried out in a number of UHV chambers with a base pressure better than 2×10^{-10} mbar. The single crystal surfaces were prepared by repeated cycles of Ar⁺ ion sputtering, followed by annealing to 740 and 670 K for the Ag(111) and the vicinal Ag(455) surface, respectively. Both precursor compounds were sublimated by OMBE from quartz glass crucibles inside Knudsen cell. The sublimation temperatures T_{OMBE} were 420 and 460 K for DETP and CN-DETP, respectively. Evaporation was carried out onto the substrates held at $T_{\text{sub}} = 300$ K or lower, whereby no covalent reactions occurred. Coupling reactions were then initiated by thermally annealing the samples via radiative heating up to the annealing temperature T_{ann} . After the preparation, the samples were cooled down and transferred into the analysis chambers for either STM or ARPES measurements.

Scanning Tunneling Microscopy: Three different STM setups were used. Low-temperature (LT-STM) data were obtained either with a custom-made Besocke-type microscope with a LHe cryostat at 5.5 K or with a commercial apparatus with a Joule-Thompson cryostat (JT-STM) fabricated by SPECS at 4.5 K. STM investigations at RT-STM were carried out in a home-built STM setup connected to a vacuum chamber also housing the PES facility, such that RT-STM and PES investigations could be conducted on the very same sample. Data were recorded with chemically etched tungsten tips in the constant current mode providing apparent height images. The bias voltage V_B was applied to the sample. If not otherwise stated, typical tunneling conditions were $V_B = \pm 0.1$ to 1 V and tunneling current $I_T = 0.1$ nA. LT-STM data obtained on the Ag(111) is displayed in a brown color coding. For LT-STM data recorded on the Ag(455) surface, instead of the apparent height the derivative along the fast scanning direction, approximately perpendicular to the step direction) is plotted with a more orange-brownish color scheme. This allows a uniform appearance of

terraces, steps, and molecular chains aligned next to the step edges despite the statistically varying width of the terraces. In the more common apparent height representation, the varying terraces width would result in confusingly different coloring of physically same features, such as a single nanowire at the edge of a small terrace versus the same nanowire at the edge of a broad terrace. RT-STM images are depicted with a black-yellow color scheme.

For conformational switching of CN-phenyl groups, the following procedure was employed. The STM images during the manipulation experiments were recorded with $V_B = -100$ mV and $I_T = 0.1$ nA for optimizing the contrast related to the CN-induced depressions. In order to perform a switching process, the tip was positioned over the center of the respective depression with the same tunneling parameters. Then, with opened feedback, the surface was approached (≈ 3 Å) until an abrupt increase in I_T took place and resulted in a I_T of several hundred nA. We attribute this increase to a conformational change of the CN-phenyl group, now pointing with the CN toward the tip and establishing a bond with it. Next, the tip is retracted by 1.5 Å, whereby a hysteresis in I_T evidences that the CN group is still experiencing the bond with the tip, and laterally moved, in constant height mode, with a speed of 1 nm s^{-1} perpendicular to the chain to the expected position of the depression resulting from the conformational switching. Finally, the feedback loop was switched on again, initiating a sudden retraction of the tip and a disruption of the bond with the CN allowing the latter to relax to its regular flat-lying configuration. Lateral manipulation of nanowire segments was carried out by positioning the tip directly above the alkyne group at the end of the chain or over a butadiyne junctions between two monomeric units with a set-point of $V_B = -100$ mV and $I_T = 0.1$ nA. While keeping the feedback loop active, the I_T was increased (typically to ≈ 30 nA) until a sudden jump in the *z*-signal occurred indicating that the chain was picked up. Then, the tip was moved to the desired position with a speed of 1 nm s^{-1} and then, retracted by reducing the set-point back to its initial value initiating the drop of the chain.

Photoelectron Spectroscopy: The PES experiments were carried out at the advanced photoelectric effect undulator beam line at the ELETTRA synchrotron facility in Trieste. The data were recorded at $T_{\text{sub}} = 77$ K utilizing a Scienta DA30 analyzer with an acceptance angle of 30° and a pass energy of 10 eV. For minimizing radiation-induced damage, the exit slits of the beam line were reduced to 20 μm . Horizontally polarized light with photon energy $h\nu = 30$ eV was used. The energy and angular resolution of the setup amounted to 20 meV and 0.2° , respectively. From the angle-resolved data, *k*-independent spectra were obtained by integrating over the full angular range. Samples were prepared in situ in UHV, employing the protocols described above. The direction of the terrace steps of the sample was aligned with the *k*-direction sampled by the analyzer to smaller than 3° , as indicated by low-energy electron diffraction (LEED). Electrons were collected with the emission direction pointing toward the center of the analyzer slit exhibiting an angle of 30° with the surface normal in order to enhance the adsorbate-related features.

Molecular Model Calculations: The models of the monomer and dimer structures utilized for superposing in Figures 1, 2, and 4 where geometry-optimized with the Hyperchem 7.5 molecular modeling package^[61] employing the semi-empirical AM1 method.

Supporting Information

Supporting Information is available from the Wiley Online Library or from the author.

Acknowledgements

This work was supported by the ERC Advanced Grant MolArt (Grant No. 247299), the TUM Institute of Advanced Studies, the Munich-Centre for Advanced Photonics, and the German Research Foundation (DFG) via KL 2294/3-1, KL 2294/6-1, and PP 1459 “Graphene.” This work had been partly performed in the framework of the Nanoscience Foundry and Fine

Analysis (NFFA-MIUR Italy) project. Measurements at the Karlsruhe Nano Micro Facility (KNMF) are acknowledged.

Conflict of Interest

The authors declare no conflict of interest.

Keywords

carbon nanomaterials, conjugated polymers, graphdiyne, information storage, on-surface synthesis

Received: December 12, 2017
Published online: February 6, 2018

- [1] R. H. Baughman, A. A. Zakhidov, W. A. de Heer, *Science* **2002**, 297, 787.
- [2] V. Singh, D. Joung, L. Zhai, S. Das, S. I. Khondaker, S. Seal, *Prog. Mater. Sci.* **2011**, 56, 1178.
- [3] S. Dutta, S. K. Pati, *J. Mater. Chem.* **2010**, 20, 8207.
- [4] L. Talirz, P. Ruffieux, R. Fasel, *Adv. Mater.* **2016**, 28, 6222.
- [5] A. L. Ivanovskii, *Prog. Solid State Chem.* **2013**, 41, 1.
- [6] Y. J. Li, L. Xu, H. B. Liu, Y. L. Li, *Chem. Soc. Rev.* **2014**, 43, 2572.
- [7] Z. Li, M. Smeu, A. Rives, V. Maraval, R. Chauvin, M. A. Ratner, E. Borguet, *Nat. Commun.* **2015**, 6, 6321.
- [8] F. Klappenberger, Y.-Q. Zhang, J. Björk, S. Klyatskaya, M. Ruben, J. V. Barth, *Acc. Chem. Res.* **2015**, 48, 2140.
- [9] M. Q. Long, L. Tang, D. Wang, Y. L. Li, Z. G. Shuai, *ACS Nano* **2011**, 5, 2593.
- [10] Y. Jiao, A. J. Du, M. Hankel, Z. H. Zhu, V. Rudolph, S. C. Smith, *Chem. Commun.* **2011**, 47, 11843.
- [11] K. Srinivasu, S. K. Ghosh, *J. Phys. Chem. C* **2012**, 116, 5951.
- [12] S. W. Cranford, M. J. Buehler, *Nanoscale* **2012**, 4, 4587.
- [13] N. L. Yang, Y. Y. Liu, H. Wen, Z. Y. Tang, H. J. Zhao, Y. L. Li, D. Wang, *ACS Nano* **2013**, 7, 1504.
- [14] G. X. Li, Y. L. Li, H. B. Liu, Y. B. Guo, Y. J. Li, D. B. Zhu, *Chem. Commun.* **2010**, 46, 3256.
- [15] J. Sakamoto, J. van Heijst, O. Lukin, A. D. Schlüter, *Angew. Chem., Int. Ed.* **2009**, 48, 1030.
- [16] A. Gourdon, *Angew. Chem., Int. Ed.* **2008**, 47, 6950.
- [17] L. Grill, M. Dyer, L. Lafferentz, M. Persson, M. V. Peters, S. Hecht, *Nat. Nanotechnol.* **2007**, 2, 687.
- [18] J. M. Cai, P. Ruffieux, R. Jaafar, M. Bieri, T. Braun, S. Blankenburg, M. Muoth, A. P. Seitsonen, M. Saleh, X. L. Feng, K. Müllen, R. Fasel, *Nature* **2010**, 466, 470.
- [19] L. Lafferentz, F. Ample, H. Yu, S. Hecht, C. Joachim, L. Grill, *Science* **2009**, 323, 1193.
- [20] J. A. Lipton-Duffin, O. Ivasenko, D. F. Perepichka, F. Rosei, *Small* **2009**, 5, 592.
- [21] G. Reecht, H. Bulou, F. Scheurer, V. Speisser, B. Carriere, F. Mathevet, G. Schull, *Phys. Rev. Lett.* **2013**, 110, 056802.
- [22] C. G. Tao, L. Y. Jiao, O. V. Yazyev, Y. C. Chen, J. J. Feng, X. W. Zhang, R. B. Capaz, J. M. Tour, A. Zettl, S. G. Louie, H. J. Dai, M. F. Crommie, *Nat. Phys.* **2011**, 7, 616.
- [23] H. M. Zhang, H. P. Lin, K. W. Sun, L. Chen, Y. Zagranyarski, N. Aghdassi, S. Duhm, Q. Li, D. Y. Zhong, Y. Y. Li, K. Müllen, H. Fuchs, L. F. Chi, *J. Am. Chem. Soc.* **2015**, 137, 4022.
- [24] Y.-Q. Zhang, N. Kepčija, M. Kleinschrodt, K. Diller, S. Fischer, A. C. Papageorgiou, F. Allegretti, J. Björk, S. Klyatskaya, F. Klappenberger, M. Ruben, J. V. Barth, *Nat. Commun.* **2012**, 3, 1286.
- [25] H.-Y. Gao, H. Wagner, D. Zhong, J.-H. Franke, A. Studer, H. Fuchs, *Angew. Chem., Int. Ed.* **2013**, 52, 4024.
- [26] J. Björk, Y.-Q. Zhang, F. Klappenberger, J. V. Barth, S. Stafström, *J. Phys. Chem. C* **2014**, 118, 3181.
- [27] B. Cirera, Y.-Q. Zhang, S. Klyatskaya, M. Ruben, F. Klappenberger, J. V. Barth, *ChemCatChem* **2013**, 5, 3281.
- [28] D. Y. Zhong, J. H. Franke, S. K. Podiyanchari, T. Blomker, H. M. Zhang, G. Kehr, G. Erker, H. Fuchs, L. F. Chi, *Science* **2011**, 334, 213.
- [29] Q. T. Fan, J. Y. Dai, T. Wang, J. Kuttner, G. Hilt, J. M. Gottfried, J. F. Zhu, *ACS Nano* **2016**, 10, 3747.
- [30] N. Kalashnyk, K. Mouhat, J. Oh, J. Jung, Y. C. Xie, E. Salomon, T. Angot, F. Dumur, D. Gimes, S. Clair, *Nat. Commun.* **2017**, 8, 14735.
- [31] T. Lin, L. Zhang, J. Björk, Z. Chen, M. Ruben, J. V. Barth, F. Klappenberger, *Chem. - Eur. J.* **2017**, 23, 15588.
- [32] B. Cirera, Y.-Q. Zhang, J. Björk, S. Klyatskaya, Z. Chen, M. Ruben, J. V. Barth, F. Klappenberger, *Nano Lett.* **2014**, 14, 1891.
- [33] F. Klappenberger, *Prog. Surf. Sci.* **2014**, 89, 1.
- [34] E. Arras, A. P. Seitsonen, F. Klappenberger, J. V. Barth, *Phys. Chem. Chem. Phys.* **2012**, 14, 15995.
- [35] J. Liu, Q. Chen, L. Xiao, J. Shang, X. Zhou, Y. Zhang, Y. Wang, X. Shao, J. Li, W. Chen, G. Q. Xu, H. Tang, D. Zhao, K. Wu, *ACS Nano* **2015**, 9, 6305.
- [36] L. Vitali, G. Levita, R. Ohmann, A. Comisso, A. De Vita, K. Kern, *Nat. Mater.* **2010**, 9, 320.
- [37] Y.-Q. Zhang, J. Björk, P. Weber, R. Hellwig, K. Diller, A. C. Papageorgiou, S. C. Oh, S. Fischer, F. Allegretti, S. Klyatskaya, M. Ruben, J. V. Barth, F. Klappenberger, *J. Phys. Chem. C* **2015**, 119, 9669.
- [38] M. Marschall, J. Reichert, K. Seufert, W. Auwärter, F. Klappenberger, A. Weber-Bargioni, S. Klyatskaya, G. Zoppellaro, A. Nefedov, T. Strunskus, C. Wöll, M. Ruben, J. V. Barth, *ChemPhysChem* **2010**, 11, 1446.
- [39] J. V. Barth, J. Weckesser, C. Z. Cai, P. Günter, L. Bürgi, O. Jeandupeux, K. Kern, *Angew. Chem., Int. Ed.* **2000**, 39, 1230.
- [40] J. Weckesser, A. De Vita, J. V. Barth, C. Cai, K. Kern, *Phys. Rev. Lett.* **2001**, 87, 096101.
- [41] D. Abbasi-Perez, J. M. Recio, L. Kantorovich, *J. Phys. Chem. C* **2014**, 118, 10358.
- [42] S. Linden, D. Zhong, A. Timmer, N. Aghdassi, J. H. Franke, H. Zhao, X. Feng, K. Müllen, H. Fuchs, L. Chi, H. Zacharias, *Phys. Rev. Lett.* **2012**, 108, 216801.
- [43] P. Ruffieux, J. M. Cai, N. C. Plumb, L. Patthey, D. Prezzi, A. Ferretti, E. Molinari, X. L. Feng, K. Müllen, C. A. Pignedoli, R. Fasel, *ACS Nano* **2012**, 6, 6930.
- [44] J. M. Cai, C. A. Pignedoli, L. Talirz, P. Ruffieux, H. Söde, L. B. Liang, V. Meunier, R. Berger, R. J. Li, X. L. Feng, K. Müllen, R. Fasel, *Nat. Nanotechnol.* **2014**, 9, 896.
- [45] Y. Zhu, H. Bai, Y. Huang, *Synth. Met.* **2015**, 204, 57.
- [46] Y. Zhu, H. Bai, Y. Huang, *ChemistryOpen* **2016**, 5, 78.
- [47] A. Damascelli, Z. Hussain, Z. X. Shen, *Rev. Mod. Phys.* **2003**, 75, 473.
- [48] L. Esaki, R. Tsu, *IBM J. Res. Dev.* **1970**, 14, 61.
- [49] A. Basagni, G. Vasseur, C. A. Pignedoli, M. Vilas-Varela, D. Peña, L. Nicolas, L. Vitali, J. Lobo-Checa, D. G. de Oteyza, F. Sedona, M. Casarin, J. E. Ortega, M. Sami, *ACS Nano* **2016**, 10, 2644.
- [50] G. Vasseur, M. Abadia, L. A. Miccio, J. Brede, A. Garcia-Lekue, D. G. de Oteyza, C. Rogero, J. Lobo-Checa, J. E. Ortega, *J. Am. Chem. Soc.* **2016**, 138, 5685.
- [51] G. Vasseur, Y. Fagot-Revurat, M. Sicot, B. Kierren, L. Moreau, D. Malterre, L. Cardenas, G. Galeotti, J. Lipton-Duffin, F. Rosei, M. Di Giovannantonio, G. Contini, P. Le Fevre, F. Bertran, L. Liang, V. Meunier, D. F. Perepichka, *Nat. Commun.* **2016**, 7, 10235.

- [52] S. Loth, S. Baumann, C. P. Lutz, D. M. Eigler, A. J. Heinrich, *Science* **2012**, 335, 196.
- [53] D. Abbasi-Perez, J. Manuel Recio, L. Kantorovich, *Phys. Chem. Chem. Phys.* **2015**, 17, 11182.
- [54] S. H. Charap, P. L. Lu, Y. J. He, *IEEE Trans. Magn.* **1997**, 33, 978.
- [55] F. Donati, S. Rusponi, S. Stepanow, C. Wäckerlin, A. Singha, L. Persichetti, R. Baltic, K. Diller, F. Patthey, E. Fernandes, J. Dreiser, Z. Sljivancanin, K. Kummer, C. Nistor, P. Gambardella, H. Brune, *Science* **2016**, 352, 318.
- [56] F. E. Kalff, M. P. Rebergen, E. Fahrenfort, J. Girovsky, R. Toskovic, J. L. Lado, J. Fernandez-Rossier, A. F. Otte, *Nat. Nanotechnol.* **2016**, 11, 926.
- [57] J. F. Lutz, M. Ouchi, D. R. Liu, M. Sawamoto, *Science* **2013**, 341, 1238149.
- [58] H. Colquhoun, J. F. Lutz, *Nat. Chem.* **2014**, 6, 455.
- [59] J. van der Lit, P. H. Jacobse, D. Vanmaekelbergh, I. Swart, *New J. Phys.* **2015**, 17, 053013.
- [60] S. Y. Wang, W. H. Wang, N. Lin, *ACS Nano* **2012**, 6, 3404.
- [61] HYPERCHEM; Hypercube Inc.: Gainesville, FL.